Magmatic Precursors of Hydrothermal Fluids at the Río Blanco Cu-Mo Deposit, Chile: Links to Silicate Magmas and Metal Transport

Paul Davidson,[†] Vadim Kamenetsky, David R. Cooke, Peter Frikken,
Center for Ore Deposit Research, University of Tasmania, GPO Box 252-79, Hobart, Tasmania, Australia

Peter Hollings,
Department of Geology, Lakehead University, Thunder Bay, Ontario, Canada P7B 5E1

Chris Ryan, Esme Van Achterbergh,
CSIRO, P.O. Box 136, North Ryde, NSW, Australia

Terry Mernagh,
Geoscience Australia, GPO Box 378, Canberra, ACT, Australia

Jorge Skarmeta,
CODELCO-Chile, Gerencia Exploraciones, Santiago, Chile

Luis Serrano, and Ricardo Vargas
CODELCO-Chile, Division Andina, Saladillo, Chile

Abstract

In most porphyry systems the obscuring effects of hydrothermal processes and subsequent alteration, along with limited exposure of source rocks, preclude a detailed understanding of how and where metals and volatiles were derived. However, in this study we examine melt inclusions which have escaped alteration and that sampled all of the phases coexisting in the magma, in late- and postmineral rhyolitic units from the Río Blanco Cu-Mo deposit, Chile. These inclusions demonstrate the existence of a volatile-rich melt, the exsolution from it of an aqueous volatile-rich phase, initially as melt + vapor bubble emulsions, and the disruption of these emulsions into melt and primary magmatic fluids. Trapping of these emulsions may explain the occurrence of melt inclusions containing widely varying proportions of melt and aqueous fluid found at Río Blanco. We demonstrate the sequestering of metals into the exsolved volatile phases and the derivation from these of possible ore-forming hydrothermal fluids, with particular reference to the implications for metal transport. Melt inclusions show differences between adjacent comagmatic intrusions that may be directly related to the extent of mineralization of the respective bodies. In one of the Río Blanco postmineral rhyolite bodies melt inclusions show exsolution of the volatile-rich phase but only minor evidence of trapping of a metal-rich vapor. In contrast, inclusions from an adjacent late mineral rhyolite body show similar volatile phase exsolution but also provide evidence of ponding of metal-rich hydrothermal fluids during the final stages of cooling.

Introduction

In magmatic-hydrothermal ore deposits, metals are sourced from silicate melt, in some cases with subsequent input of metals remobilized by meteoric fluids (e.g., Hedenquist and Lowenstern, 1994). Given that base and precious metals strongly partition from silicate melts into volatile-rich phases (e.g., Candela and Holland, 1984; Lowenstern et al., 1991; Candela and Piccoli, 1995; Harris et al., 2003), it is crucial to understand the process of exsolution of volatiles. Immiscible separation of melt and volatile phases is probable at some point in the evolution of many felsic magmas, given the typical concentrations of H_2O in silicate melts. However, various factors such as initial melt composition and the physical parameters of emplacement, crystallization, and degassing mean that each intrusion should differ in the temperature of exsolution, the amount and compositions of immiscible

phases exsolved, and the efficiency of extraction (e.g., Cline and Bodnar, 1991). The process of mineralization is evidence of the separation of volatiles and ore-forming elements from the residual magma and migration of the ore-forming elements (in whatever form) away from their source. If this separation is efficient, then the residual magma can be assumed to be significantly depleted in volatiles and metals relative to the parental magma but to an unknown extent. Thus, the cooled and crystallized source rocks should contain little evidence of their original metal and volatile content and the means by which they escaped from the magma, leaving no way to reconstruct them. One exception may be any melt inclusions that were trapped in crystallizing minerals during exsolution (e.g., Roedder, 1984; Lowenstern, 1995; Frezzotti, 2001; Kamenetsky et al., 2003). These provide critical evidence of the processes of volatile exsolution and the sequestering, transport, and ultimate deposition (or nondeposition) of metals.

[†] Corresponding author: e-mail, paul_d@postoffice.utas.edu.au

As an example of the information that can be obtained from melt inclusions, we present new data from the giant Río Blanco-Los Bronces Cu-Mo deposit. The rocks used in this study come from the late mineral Don Luis Porphyry (5.23 ± 0.07 Ma.) and postmineral La Copa rhyolite, (4.03 ± 0.19 Ma., Deckart et al., 2005). Both are rhyolitic intrusive bodies, the latter with extrusive equivalents. Although late in the mineralizing sequence, these rocks show geochemical, temporal, and spatial continuity with the main mineralization events. It will be shown that processes that occurred in the original magmas also can be related to the mineralization events.

In an earlier study (Davidson and Kamenetsky, 2001), we proposed immiscibility between two silicate melts, one of which was volatile rich and that this volatile-rich melt was a source of aqueous fluids during later evolution, and we described the melt and fluid inclusions occurring in the Don Luis Porphyry and intrusive units of the La Copa rhyolite. In this study, we also examine the extrusive equivalents of the La Copa rhyolite, which contain composite inclusions and textures that were not observed in the intrusive samples. Additionally, proton induced X-ray emission (PIXE) microprobe analyses and fluid inclusion microthermometry have now been performed on both the intrusive and extrusive suites. These new data expand the earlier published results and allow new constraints on the nature of fluid phase exsolution in the studied suites. In particular, we provide evidence of the trapping of emulsions of silicate melt and bubbles of aqueous liquid and vapor as melt inclusions. These emulsions are most clearly observed in the extrusive rocks, possibly due to quenching. However, we will show that the same materials may have been trapped in the intrusive equivalents, although the characteristic textures were subsequently destroyed by crystallization of the inclusions. The newly observed magmatic emulsions now provide an alternative explanation to that proposed in Davidson and Kamenetsky (2001); specifically, that magmatic emulsions may provide a connecting link between saturated silicate melts and exsolved hydrothermal fluids.

The magmatic emulsions (silicate melt, now glass, with entrained aqueous fluid bubbles) and their crystallized equivalents, permit the analysis of pristine examples of primary magmatic fluids, unaffected by mixing and contamination that occurs during transport out of the magma chamber. With this information we are able to describe in some detail the long accepted but poorly documented processes of volatile exsolution from a felsic melt.

Regional and Local Geology

The Río Blanco and Los Bronces mines exploit one of the world's largest porphyry-related copper-molybdenum deposits (70 million metric tons (Mt) at 0.75% copper and 0.02% molybdenum: Camus, 2002). The mines are operated by CODELCO (Río Blanco) and Anglo American (Los Bronces) and are located approximately 70 km northeast of Santiago (Fig. 1A). The ore deposit, hereafter referred to as Río Blanco, forms part of the late Miocene-Pliocene metallogenic province of central Chile. This province also contains the giant copper-molybdenum deposits at El Teniente (Cannell et al., 2005) and Los Pelambres (Atkinson et al., 1996).
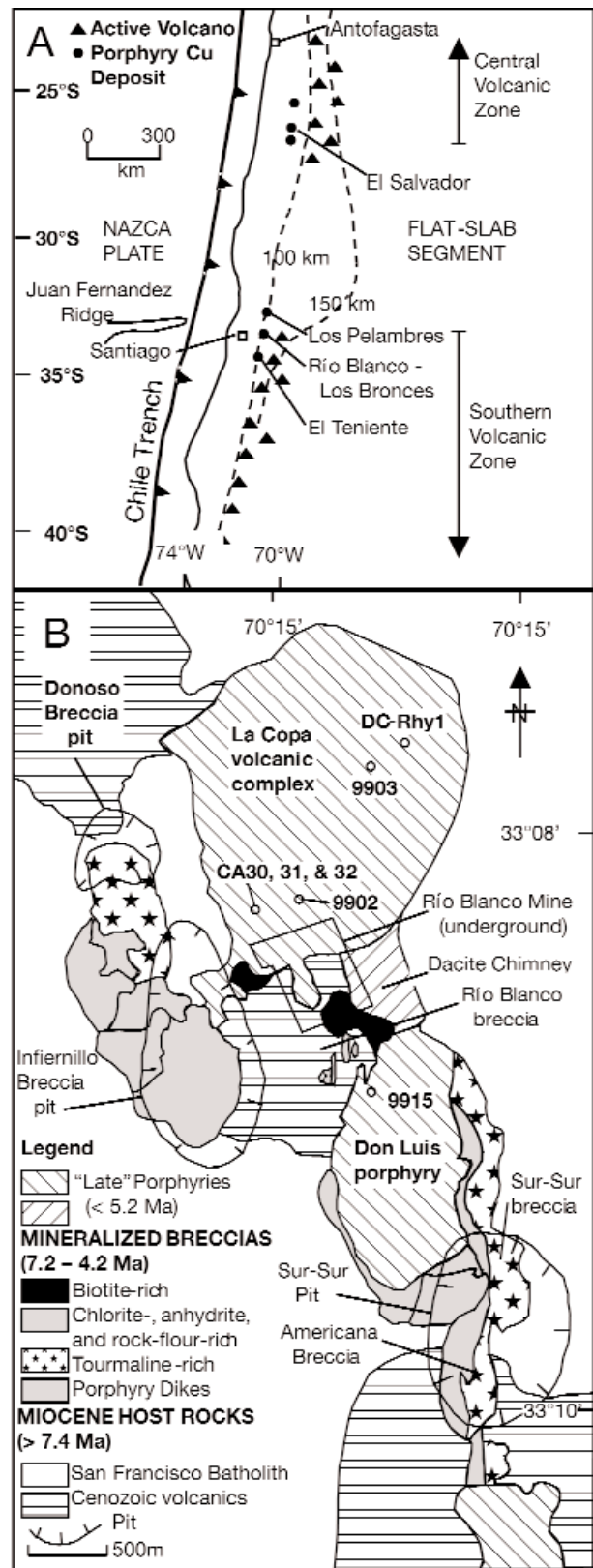

Fig. 1. Maps of Río Blanco. A. Location map showing major porphyry copper deposits in relationship to the flat-slab section of the Chilean subduction zone (contours are depth to the subducted oceanic lithosphere, after Serrano et al., 1996). B. Geology of the Río Blanco-Los Bronces deposit, after Vargas et al. (1999). Sample locations are indicated.

The Río Blanco deposit is hosted partly within a Miocene batholith (San Francisco batholith) that intruded weakly deformed Tertiary volcano-sedimentary sequences (the Abanico and Farellones Formations). The regional geology and tectonic evolution of central Chile are described in Hollings et al. (2005) and references therein. Deckart et al. (2005) provide new geochronology of the Miocene host rocks.

Río Blanco is atypical of many porphyry deposits in that ore is hosted primarily within biotite- and tourmaline-cemented breccias (Waarnars et al., 1985; Serrano et al., 1996; Vargas et al., 1999; Frikken et al., 2005). These large breccia Complexes are highly fragmented, commonly heterolithologic, and show multiple phases of explosive fracturing (Vargas et al., 1999) and have been intruded by a sequence of weakly mineralized and altered quartz monzonite, dacite, and rhyolite porphyries during the late Miocene and early Pliocene (the "late porphyries" of Serrano et al., 1996, and Deckart et al, 2005; Table 1, Fig. 1B). The strongly mineralized biotite- and tourmaline-cemented breccias appear to be most closely related to the Quartz Monzonite Porphyry and Feldspar Porphyry intrusions and a close genetic relationship is inferred (Frikken, 2004; Deckart et al., 2005; Frikken et al., 2005; Table 1). Subsequent to the formation of the mineralized breccias, a series of weakly altered and mineralized to barren subvolcanic intrusions were emplaced at Río Blanco. These are, in chronological order, the Don Luis Porphyry, Dacite Chimney, and La Copa Complex, which form a northward projection through time that has cut primary breccia-hosted mineralization (Table 1, Fig. 1B). These intrusions typically have mechanically brecciated contact zones, some of which have been cemented by tourmaline, sulfides, and rock flour (Serrano et al., 1996). We have found workable melt inclusions in the Don Luis Porphyry and within intrusive and extrusive units of the La Copa Complex. These units are described in more detail below.

The dacitic Don Luis Porphyry has cut mineralized tourmaline breccia in the La Unión and Don Luis sectors of the Río Blanco mine (Fig. 1B). The wall rocks adjacent to the Don Luis Porphyry were brecciated during the intrusive event ("emplacement" breccia of Serrano et al., 1996). The Don Luis Porphyry has been cut locally by veins of quartz ± sericite ± anhydrite ± sulfide and by K-feldspar veins (Table 1). Up to 0.6 percent copper has been detected in this unit but copper grades are mostly below 0.5 percent (Frikken, 2004). Some of the contacts between the Don Luis Porphyry and adjacent wall rocks have been altered to a quartz-sericite assemblage.

The Dacite Chimney was emplaced to the north of and postdated the Don Luis Porphyry and consists of a dacitic to quartz latite porphyry in the shape of an inverted cone (Frikken, 2004). Along its perimeter, the Dacite Chimney contains a discontinuous rim of emplacement breccia with a cement stained by iron oxides with less common primary specularite, chlorite, and sulfide minerals (Frikken, 2004). Although copper grades are low in the Dacite Chimney (<0.3% Cu) and in the emplacement breccia, the emplacement breccia appears to have been the focus for late-stage fluid flow and minor copper deposition (Frikken, 2004). The Dacite Chimney does not contain stockwork veins typical of porphyry copper environments.

TABLE 1. Characteristics of the Late Porphyries at Río Blanco-Los Bronces

Unit	Composition and form	Age	Alteration minerals	Veins	Melt inclusions[1]	References
La Copa Complex	Dacitic volcanic breccias, ignimbrite, tuff, dacite dikes, minor andesite	4.03 ± 0.19 (K-Ar biotite)	Weak sericite alteration locally	Fragments of mineralized breccia, mineralized andesite, and mineralized quartz monzonite are present in the diatreme	Yes	Quirt et al. (1971), Waarnars et al. (1985), Torros George (1986), Deckart et al. (2005)
Río Blanco dacite plug (dacite chimney)	Dacite and quartz latite porphyry (<0.3% Cu)	4.92 ± 0.09 (SHRIMP zircon)	Weak quartz-sericite alteration	Contact zone emplacement breccia has a chlorite-specularite-biotite cement with minor chalcopyrite	No	Waarnars et al. (1985), Serrano et al. (1996), Frikken (2004), Deckart et al. (2005)
Don Luis porphyry	Plagioclase-orthoclase-quartz-phyric dacite with minor biotite (≤0.6% Cu)	5.23 ± 0.07 (TIMS U-Pb)	Quartz-sericite alteration (feldspars altered to sericite; primary biotite altered to chlorite)	Quartz-molybdenite ± chalcopyrite veins; quartz ± sericite ± anhydrite ± sulfide (D) veins; minor K-feldspar veins	Yes	Frikken (2004), Deckart et al. (2005)
Feldspar porphyry	Plagioclase-megacrystic orthoclase-quartz-biotite-phyric quartz monzonite	5.84 ± 0.03 (TIMS U-Pb)	Sericite alteration of feldspars; chlorite alteration of primary biotite; rare vein halos of biotite, magnetite, and minor chalcopyrite	Quartz-anhydrite-chalcopyrite ± biotite ± tourmaline ± bornite ± specularite veins with biotite halos; quartz ± sericite ± anhydrite ± sulfide (D) veins with sericite halos	No	Frikken (2004), Deckart et al. (2005)
Quartz monzonite porphyry	Plagioclase-megacrystic orthoclase-quartz-biotite-phyric quartz monzonite dikes	6.32 ± 0.09 (TIMS U-Pb)	Quartz-sericite, chlorite, silcification	Quartz ± sericite ± anhydrite ± sulfide (D) veins with sericite halos; minor K-feldspar veins	No	Serrano et al. (1996), Frikken (2004), Deckart et al. (2005)

Notes: D veins refer to pyrite-rich veins with sericite-quartz-pyrite alteration halos, akin to the D veins described from El Salvador by Gustafson and Hunt (1975)
[1] Melt inclusions are preserved in quartz and feldspar phenocrysts in the La Copa Complex and the Don Luis porphyry

The La Copa Complex was emplaced during the final phases of magmatism at Río Blanco. Extrusive rocks (rhyolitic lavas, ignimbrites, and tuffs) crop out in the southwestern part of the La Copa Complex at high altitudes in the Los Bronces area (Fig. 1B), indicating that the orebody had been partly exhumed by the time the La Copa Complex was emplaced. At least seven discrete intrusive phases of dacitic to rhyolitic composition have been mapped within the La Copa Complex (Toro, 1986). There is also an unmineralized diatreme which most likely formed by explosive phreatomagmatic activity late in the evolution of the ore system (Serrano et al., 1996). The La Copa intrusive units and diatreme breccia form an inverted cone-shaped body that has truncated mineralized breccias in the Río Blanco orebody, as shown in the geologic cross sections of Deckart et al. (2005) and Frikken et al. (2005). CODELCO recently discovered high-grade ore by underground drilling in marginal breccias around the La Copa Complex, although no ore has yet been found in the La Copa Complex itself. Weak sericite alteration has been noted in several units (Toro, 1986). As with the Dacite Chimney, the La Copa Complex does not contain a stockwork of veins typical of porphyry copper environments.

Sample Descriptions

The La Copa intrusive units sampled in this study (DC-Rhy1, 9902, and 9903; Fig. 1B, Table 2) are plagioclase + quartz ± biotite-phyric rhyolites with sparse fine-grained igneous xenoliths, some of which may be mesocratic microgranular enclaves. All the samples are fresh, with only minor sericite alteration. The extrusive units in this study (CA30, CA31, CA32; Fig. 1B, Table 2) are glass-bearing porphyritic plagioclase + quartz + biotite-phyric rhyolite lavas, also containing small igneous xenoliths. Only weak sericitic and chloritic alteration has been noted. Samples CA31 and CA32 were collected directly above paleosol horizons indicating that they are extrusive in origin. Whole-rock analyses are provided in Table 2.

The Don Luis Porphyry sample analyzed in this study (9915; Fig. 1B, Table 2) is a mineralized quartz-feldspar-biotite-phyric rhyolite, showing some alteration. Much of the feldspar is sericitized and much of the biotite chloritized. Pyrite and minor chalcopyrite are noted in this sample (total sulfur in the unrecalculated analysis of sample 9915 was 4.69 wt %).

Methods

Major element analyses of inclusions in this study were performed on the Cameca SX50 electron microprobe at the Central Science Laboratory, University of Tasmania. Because of the small size of the inclusions and the common occurrence of shrinkage bubbles, we used a small, 5μm-diam beam. However, this is likely to produce problems of time-dependent loss of Na (Morgan and London, 1996). To reduce alkali diffusion problems, Na and Si concentrations were measured

TABLE 2. Whole-Rock XRF Analyses and Average Glass Inclusion Compositions by Electron Microprobe

Whole rock	9915	DC-Rhy1	9902	CA30	CA31	CA32
SiO_2	70.62	72.12	71.82	70.78	70.59	70.90
TiO_2	0.23	0.18	0.19	0.21	0.20	0.25
Al_2O_3	16.33	15.91	16.09	16.72	16.97	16.75
$FeO_{(tot)}$	2.26	1.21	1.30	1.41	1.58	1.62
MnO	0.01	0.02	0.05	0.04	0.02	0.02
MgO	0.48	0.42	0.48	0.44	0.67	0.63
CaO	0.71	2.09	2.07	2.35	2.26	2.27
Na_2O	4.24	5.26	4.88	5.27	5.05	3.87
K_2O	5.02	2.72	3.03	2.71	2.59	3.59
P_2O_5	0.10	0.07	0.07	0.07	0.08	0.09
Total	100.00	100.00	100.00	100.00	100.00	100.00

Glass inclusions	9903	1σ	DC-Rhy1	1σ	CA30	1σ	CA31	1σ	CA32	1σ
SiO_2	72.12	1.41	72.08	1.30	71.93	0.56	72.05	0.58	73.30	0.73
TiO_2	0.06	0.01	0.06	0.01	0.06	0.02	0.07	0.02	0.07	0.03
Al_2O_3	13.22	0.58	13.39	0.53	12.96	0.35	12.97	0.19	13.41	0.27
$FeO_{(tot)}$	0.13	0.11	0.15	0.09	0.26	0.08	0.32	0.10	0.35	0.04
MnO	0.03	0.02	0.04	0.03	0.04	0.02	0.04	0.02	0.02	0.02
MgO	0.01	0.02	0.02	0.01	0.05	0.02	0.04	0.02	0.04	0.02
CaO	0.49	0.09	0.51	0.05	0.49	0.04	0.49	0.03	0.55	0.08
Na_2O	5.41	0.73	5.18	0.46	3.14	0.54	3.41	0.77	5.09	0.27
K_2O	4.26	0.59	4.66	0.48	6.19	0.52	5.82	0.59	4.34	0.24
P_2O_5	0.03	0.02	0.02	0.02	0.02	0.01	0.02	0.01	0.03	0.02
Cl	0.05	0.02	0.05	0.02	0.05	0.04	0.06	0.02	0.04	0.01
Total	95.56		95.95		95.53		95.54		97.10	

Notes: Samples DC-Rhy1, 9902, and 9903 are intrusive and CA30 through CA32 are extrusive units of the La Copa Complex, 9915 is an intrusive unit from the Don Luis porphyry; whole-rock analyses are recalculated to zero LOI; sample 9915 is also recalculated to zero sulfides; to compensate for alkali-diffusion effects all electron microprobe data have been corrected for Na loss and Si and Al grow in (Morgan and London, 1996)

simultaneously, using different spectrometer crystals, before the other elements. The beam current used was 25 nA with an acceleration voltage of 15 kV. Where inclusions were large enough, two or three spots were analyzed in each inclusion and the result given as an average. Additionally, analyses of an obsidian standard using different beam diameters were used to determine an empirical correction factor for the Na loss (Morgan and London, 1996), and microprobe data is presented in corrected form.

Individual phases in melt inclusions were identified with an Oxford Link Pentafet SATW energy dispersive X-ray detector attached to an ElectroScan ESEM2020 environmental scanning electron microscope (Central Science Laboratory, University of Tasmania). The environmental scanning electron microscope was used for imaging of exposed melt inclusions. A Dilor SuperLabram Laser Raman microprobe (GeoScience Australia, Canberra) was used to identify mineral phases, particularly in fluid inclusions. Proton-induced X-ray emission (PIXE) analyses were performed on the CSIRO-GEMOC nuclear microprobe (North Ryde, Australia), using a 0.6-nA beam of 3-MeV protons focused into a 1.3-μm beam spot. PIXE data are presented both as absolute concentrations and gray-scale element concentration maps.

Description of Inclusions

Inclusions of microphenocrysts, glass, crystallized silicates, a variety of aqueous fluids, and various combinations of these (i.e., in composite inclusions) have been found in quartz and feldspar phenocrysts from the La Copa rhyolite. These inclusions have a random distribution but are typically concentrated in growth planes (Fig. 2A). The Don Luis Porphyry contains similar populations of inclusions, except that glass inclusions are absent, and hypersaline multiphase fluid inclusions, which are absent in the La Copa rhyolite, are abundant. Davidson and Kamenetsky (2001) previously described the inclusion types present in intrusive units of the La Copa rhyolite and the Don Luis Porphyry. The extrusive units of the La Copa rhyolite have populations of glass, vapor, and crystallized silicate melt inclusions similar to those in the extrusive units, but they contain varieties of composite inclusion not previously described. The descriptions of inclusions presented here are primarily concerned with the inclusions in the La Copa extrusive units (CA30-CA32).

Silicate inclusions

Glass inclusions from the La Copa rhyolite (CA30-CA32, DC-Rhy1, 9902, and 9903) characteristically have rounded negative crystal shapes (Fig. 2B) and typically range from 1 to 50 μm in diameter, containing clear glass, shrinkage bubble(s), ±daughter crystals, typically quartz (identified by electron microprobe analyses). Shrinkage bubbles are almost invariably spherical and are typically large, averaging 6 ± 2 vol percent (1σ) of the inclusion. However, examples have been noted in which bubbles occupy a much larger relative volume (up to 100%, Fig. 2C), and these probably represent co-trapped vapor. Similar examples are described by Frezzotti (2001) and Lowenstern (1995).

In addition to glass inclusions, many of the inclusions in all of the Río Blanco rhyolites are crystallized. In transmitted light they characteristically have distinct domains, with dark and clear areas occurring in irregular zones or patches (Fig. 2D), but they are white when viewed in reflected light. Such inclusions have the same shapes and size range as glass inclusions but consist of crystalline masses separated by irregular, crystal-lined cavities (Fig. 2E-F). In transmitted light, these cavities show up as black areas and the crystalline masses as white and/or translucent patches. Davidson and Kamenetsky (2001) demonstrated that this type of inclusion, found in all Río Blanco samples and previously referred to as type 2 inclusions, were, in fact, crystallized from a trapped melt not devitrified or resulting from postmagmatic alteration. In this paper, we now use the more descriptive term "crystallized silicate melt inclusion."

Cavities in crystallized silicate melt inclusions are lined with euhedral silicate crystals, primarily feldspars, quartz, and micas and rare halite, sphalerite, chalcopyrite, Fe-Ti oxides, calcite, and siderite (Fig. 2E). Due to their highly irregular shapes, the percentage of cavity in a given inclusion is difficult to measure accurately, but we estimate that the inclusions show a continuous range from >90 vol percent (Fig. 2D-E) to <10 percent silicates (i.e., vapor-rich inclusions containing minor silicates: Fig. 2C, F). Unhealed or partly healed decrepitation cracks are a common feature of crystallized silicate melt inclusions, as are discontinuous halos of small, vapor-rich fluid inclusions (Fig. 2D).

Fluid inclusions

Primary, vapor-rich inclusions are common in all samples from the La Copa rhyolite and Don Luis Porphyry, typically occurring in growth planes randomly mixed with silicate inclusions. In transmitted light, primary vapor inclusions are dark, with negative crystal shapes, and typically ≈50 μm in diameter (Fig. 2C). When exposed, such inclusions can be seen to be smooth-walled cavities, some of which are lined with a small amount of silicate crystals (Fig. 2F). Rare halite crystals also have been observed. These vapor-rich inclusions constitute one end member of the crystallized silicate melt inclusions, which range from silicate to vapor rich (e.g., Fig. 2E-F).

Rare examples of primary, two-phase liquid-rich fluid inclusions have been identified in intrusive units of the La Copa rhyolite (samples 9902 and 9903, Fig. 3A). Laser Raman analysis confirms that they contain water, and there is no evidence of cracks or fractures through which these inclusions may have refilled. Figure 3A shows an example of such an inclusion in a growth plane with a large crystallized silicate melt inclusion. Although the inclusion resembles a glass inclusion, it has the Raman spectra for liquid water, and smaller examples show Brownian motion of the bubbles. Similar two-phase magmatic aqueous liquid-filled inclusions have been described by Naumov et al. (1992, 1994) in phenocrysts from rhyolites in Slovakia and central Tien Shan.

Quartz phenocrysts in the sample from the Don Luis Porphyry (9915) contains abundant multiphase fluid inclusions (e.g., Fig. 3B), which contain an aqueous liquid, several transparent crystals (including halite, sylvite and anhydrite), a vapor bubble, and commonly one or more opaques (chalcopyrite and titanomagnetite). It should be noted that hypersaline fluid inclusions are not found in any samples from the La Copa rhyolite. The number of phases in each inclusion
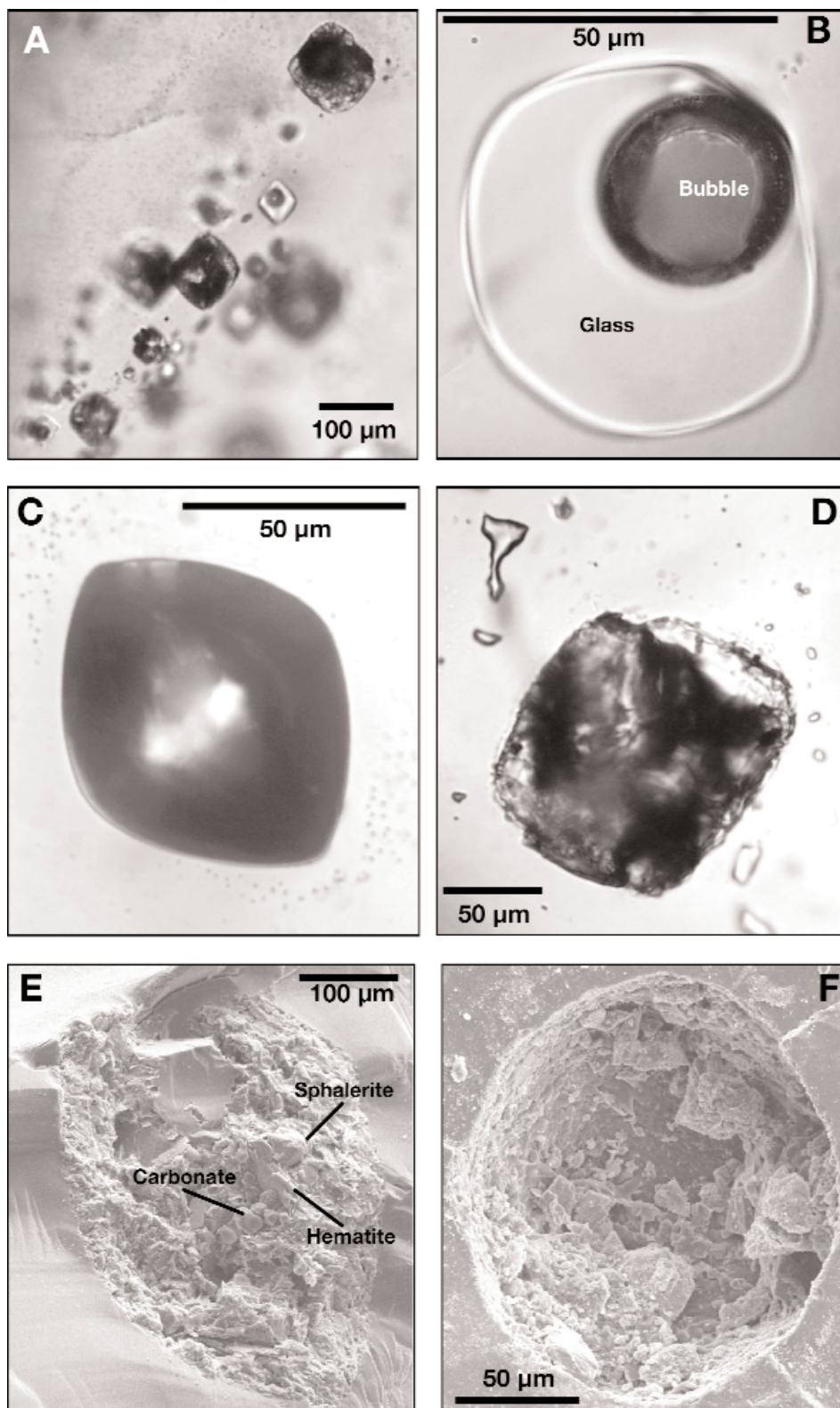
FIG. 2. Representative inclusions in quartz phenocrysts from intrusive units of the La Copa rhyolite. A. Growth plane decorated with glass and crystalline silicate melt inclusions (sample 9902). B. A typical glass inclusion with a large shrinkage bubble (DC-Rhy1). C. A primary magmatic vapor-rich inclusion (DC-Rhy1). D. Crystallized silicate melt inclusion, showing a decrepitation halo of tiny vapor inclusions (sample 9903). E. Electron photomicrograph of an opened crystallized silicate melt inclusion containing small sphalerite, hematite, and carbonate crystals in a matrix of quartz, feldspar and minor muscovite (DC-Rhy1). F. Electron photomicrograph of an opened vapor-rich inclusion containing only a small quantity of quartz and feldspar crystals (sample 9902). Originally, this inclusion would have resembled Figure 2C before it was exposed.
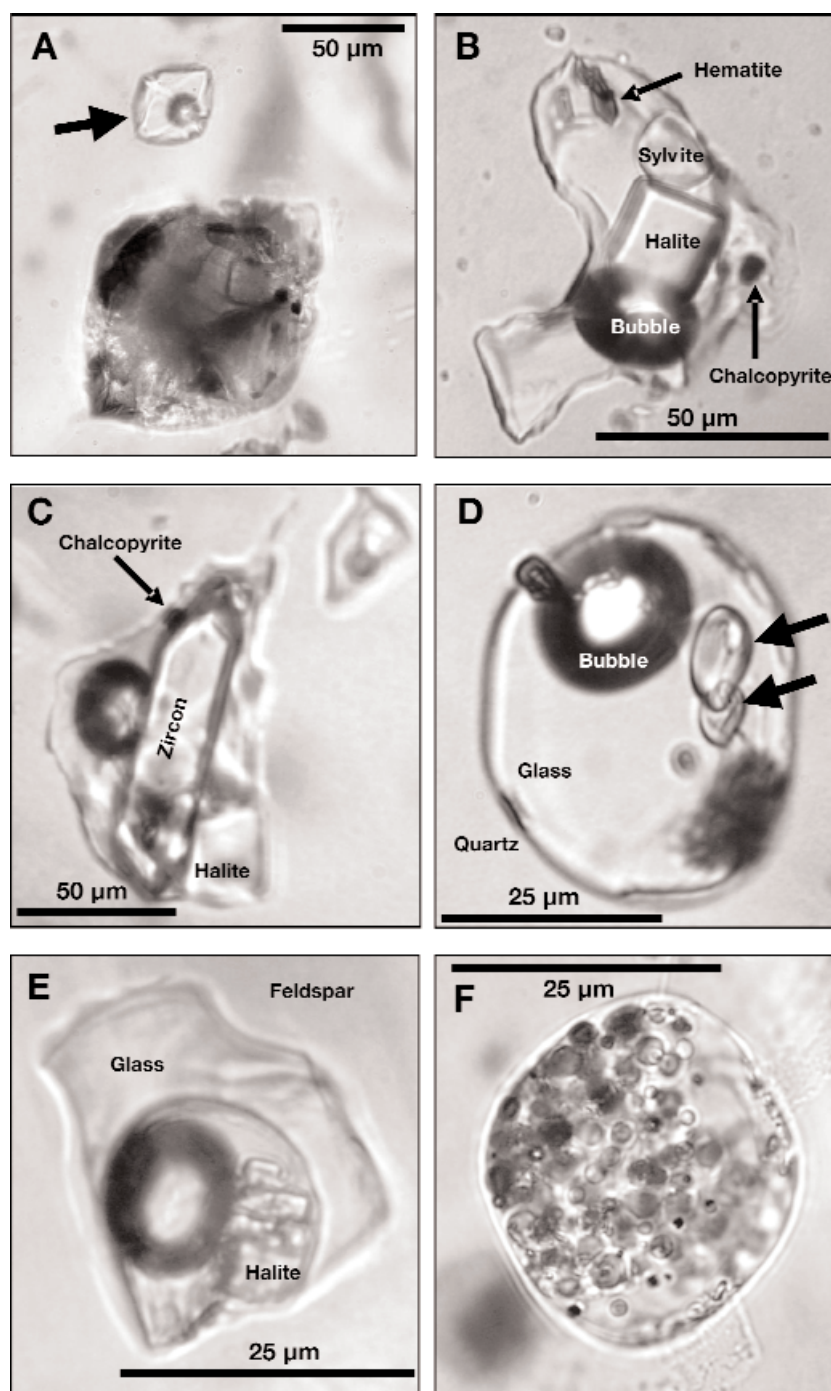
FIG. 3. Photomicrographs of melt and fluid inclusions from Rio Blanco phenocrysts, minerals were identified optically or by Laser Raman microprobe. A. Primary magmatic two-phase aqueous fluid inclusion (arrow) in a growth plane with a large crystallized silicate melt inclusion. Inclusions in a quartz phenocryst from the La Copa intrusions (sample 9902, (Davidson and Kamenetsky, 2001). This fluid inclusion appears similar to a glass inclusion, but Laser Raman analysis shows it contains liquid water, and Brownian motion of the bubbles is noted in smaller inclusions in the same trail. B. Hypersaline fluid inclusion, containing halite, sylvite, chalcopyrite, and a hematite blade. Inclusion is in a quartz phenocryst from the Don Luis Porphyry (sample 9915). C. Fluid inclusion containing various salts, a chalcopyrite crystal (arrow) and a large zircon crystal; inclusion is in a quartz phenocryst from the Don Luis Porphyry (sample 9915, Davidson and Kamenetsky, 2001). D. A composite inclusion containing glass and aqueous fluid, the glass contains a large shrinkage bubble and two single-phase aqueous bubbles (arrows). Note the deformed shape of the liquid-filled bubbles in comparison to the almost spherical vapor bubble. These liquid-filled bubbles freeze into a mass of tiny ice crystals at temperatures below 0°C, showing that they are in fact aqueous liquid rather than daughter minerals. Inclusion is in a quartz phenocryst from the La Copa lava (CA30). E. Composite inclusion containing a bubble of aqueous liquid with abundant halite, enclosed in glass in a feldspar microphenocryst in La Copa lava (CA30). F. A composite inclusion containing multiple vapor bubbles in a matrix of glass. Inclusion is in a quartz phenocryst from the La Copa lava (CA30). Note the variable proportion of aqueous fluids in inclusions D to F.

ranges from three to ten. Rare inclusions contain a single halite crystal occupying ≥90 vol percent of the inclusion. The morphologies of the inclusions range from lenticular forms with strongly cuspate margins to equant globular forms. Although many of the fluid inclusions in the Don Luis Porphyry appear to be secondary (being aligned in planes that crosscut the phenocrysts), rare hypersaline fluid inclusions can be found in growth planes, where multiphase fluid inclusions coexist with crystallized silicate melt inclusions. Additionally, some multiphase fluid inclusions contain crystals of magmatic minerals, either apatite, zircon (Fig. 3C), feldspar, or muscovite. Zircon and apatite crystallize at temperatures too high and are present in concentrations too large, to have grown from solution after trapping. The crystals do not penetrate the host and can be accounted for only if they were cotrapped with the fluid, thus implying that discrete phenocrysts of magmatic minerals coexisted with the aqueous fluids at the time of trapping.

Composite inclusions

In this paper the term composite inclusion refers to a single inclusion that contains two or more of glass, crystallized silicates, or an aqueous phase, which also occur elsewhere in the sample as separate inclusions. Davidson and Kamenetsky (2001) described composites of glass and crystallized silicate melt from the La Copa intrusive units (DC-Rhy1, 9902, and 9903). Similar inclusions have since been discovered in the La Copa intrusive units (CA30-CA32). These inclusions consist of clear glass, with or without the shrinkage bubbles and daughter crystals, with clearly defined globules of crystalline silicates, similar to crystallized silicate melt inclusions (Fig. 4C). The proportion of glass and crystallized silicates varies widely between such inclusions. When exposed by polishing, globular crystalline masses are found to contain a mass of intergrown micron-scale silicate crystals lining a random honeycomb of interstitial cavities and thus have all of the characteristics of crystallized silicate melt inclusions. Electron microprobe analysis of the glass in the composite inclusions has revealed compositions similar to the average values for glass inclusions in the same sample and within the range of compositions of such inclusions (Table 2). Laser Raman spectra for the dark globules in the composite inclusions confirm the presence of muscovite and feldspars, as in crystallized silicate melt inclusions.

In addition, the La Copa lavas (CA30-CA32) contain inclusions that typically consist of clear glass, with or without shrinkage bubbles and daughter crystals, with clearly defined liquid- or vapor-filled bubbles (Figs. 3D-F, 5A-B). Composite inclusions are rare, typically <<1 percent of the combined glass and crystallized silicate melt inclusion populations.

Composite inclusions of glass and aqueous liquid have been found so far only in the samples of La Copa rhyolite lavas collected for this study and have not been previously described. At room temperature, aqueous fluid occurs as distinct, clearly defined bubbles, containing liquid water (e.g., Figs. 3D, 5A) with or without solid crystalline phases, such as Fe-Ti oxides and halite (Fig. 3E), or water vapor. Freezing experiments (Fig. 5A-B) demonstrate that the bubbles contain aqueous liquid. Some inclusions contain only one or more bubbles of a single phase (Fig. 5A), but some contain randomly mixed bubbles of aqueous liquid, vapor, or both (Fig. 3D-F). Characteristically, the volume of the bubbles or globules varies widely, relative to the total volume of the inclusion. The presence of multiple bubbles is common (Fig. 3F). Vapor or shrinkage bubbles in this type of composite inclusion are typically spherical (e.g., Fig. 2B), but one- and two-phase fluid-filled bubbles are commonly elongated and appear deformed or stretched (e.g., Fig. 3D). Examples are noted in which multiple bubbles in the same inclusion appear to be deformed in parallel arrays. This suggests plastic deformation of the melt that contained the liquid-filled bubbles.

Although we have shown by Laser Raman spectroscopy and microthermometry that the bubbles contain a single-phase aqueous liquid, their presence appears anomalous, given that the inclusions have cooled from magmatic temperatures, and we will propose a tentative explanation in the discussion.

Microthermometry

Silicate inclusions

Heating to temperatures as high as 1,100°C over periods of up to 96 hrs failed to homogenize the glass inclusions or large (>10-μm) crystallized silicate melt inclusions, although complete or partial melting without disappearance of the shrinkage bubble commonly occurred. The failure of these inclusions to homogenize was probably due to decrepitation. This would explain the large shrinkage bubbles in glass inclusions, which average 6.0 vol percent, exceeding the suggested range of 0.1 to 5.0 vol percent for shrinkage bubbles in felsic melts (Lowenstern, 1995, 2003). However, homogenization of small crystallized silicate melt inclusions at 820° to 850°C demonstrates that they trapped a homogeneous phase, and this provides an estimate of the trapping temperature in the La Copa rhyolite.

Fluid inclusions

Multiphase fluid inclusions in quartz phenocrysts from the Don Luis Porphyry (Table 3) homogenize by both halite dissolution (avg T_h 462°C; 1σ = 54°C) and bubble disappearance (avg T_h 385°C; 1σ = 79°C), with a range of homogenization temperatures for all fluid inclusions from 165° to more than 600°C (the upper limit for the fluid inclusion stage used). An average salinity of 56 ± 5 (1σ) wt percent $NaCl_{equiv}$ is calculated using the techniques of Bodnar and Vityk (1994). Petrographic evidence suggests that trapping of the hypersaline fluid inclusions in the Don Luis Porphyry occurred under subcritical conditions. Homogenization by halite dissolution, and the presence of inclusions with >85 wt percent NaCl suggest that in some cases the fluid was probably supersaturated (Roedder, 1984). Given the low trapping pressure, probably <0.5 kbars (Holmgren et al., 1988; Vargas et al., 1999), the homogenization temperatures for these inclusions are a reasonable approximation of the trapping temperatures. Thus, the inferred trapping temperatures for hypersaline inclusions range from 340° to at least 600°C. However, the petrographic evidence cited above and the microthermometry suggests that trapping may have occurred from 600°C to magmatic temperatures (820°–850°C, for the crystallized silicate melt inclusions).
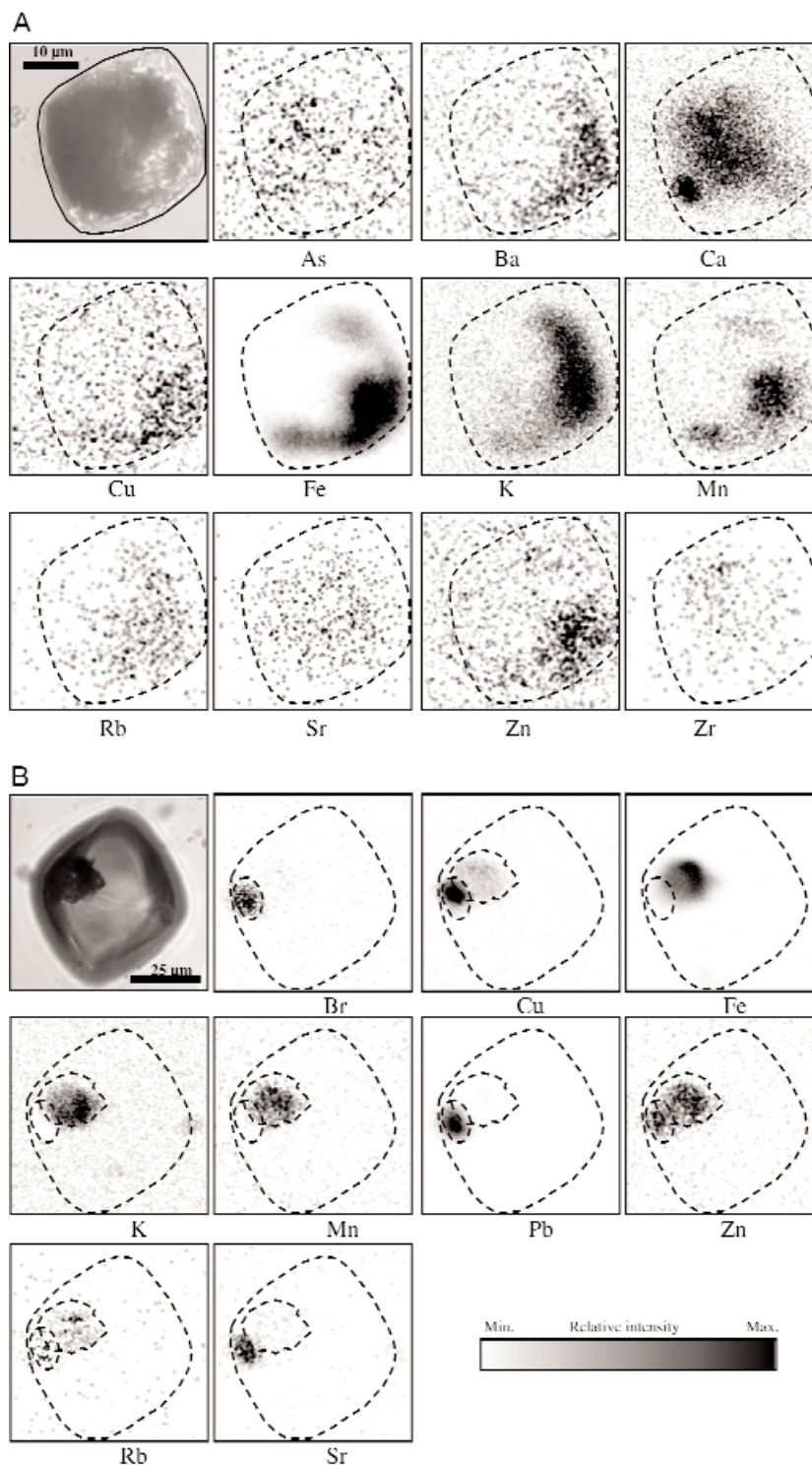
FIG. 4. Proton induced X-ray emission (PIXE) microprobe element concentration maps of inclusions in quartz phenocrysts from Rio Blanco. The element maps are gray-scale relative concentration images, normalized to the highest concentration in each map. Dashed lines correspond to the outline of the inclusion. A. Crystallized silicate melt inclusion intermediate between silicate and vapor rich (BM31, Table 4). The inclusion is from an intrusive unit of the La Copa rhyolite (sample 9902). B. Vapor-rich inclusion (BM43, Table 4), showing two distinct regions in this inclusion, one enriched in Br, Cu, Pb, and Sr, possibly a sulfide, the other enriched in Fe, K, and Mn, possibly a silicate. The inclusion is from an intrusive unit of the La Copa rhyolite (DC-Rhy1). C. Composite inclusion containing glass and crystalline silicate melt (BM41). The glass body of the inclusion contains a shrinkage bubble (left, circular) and an attached body of crystallized silicate material. The inclusion is from an extrusive unit of the La Copa rhyolite (CA31). D. Multiple-bubble, composite inclusion of glass and primary aqueous liquids, showing a microemulsion texture (BM48, Table 4). Dark bubbles are vapor, and clear bubbles are one- or two-phase aqueous fluids. The inclusion is from an extrusive unit of the La Copa rhyolite (CA31).
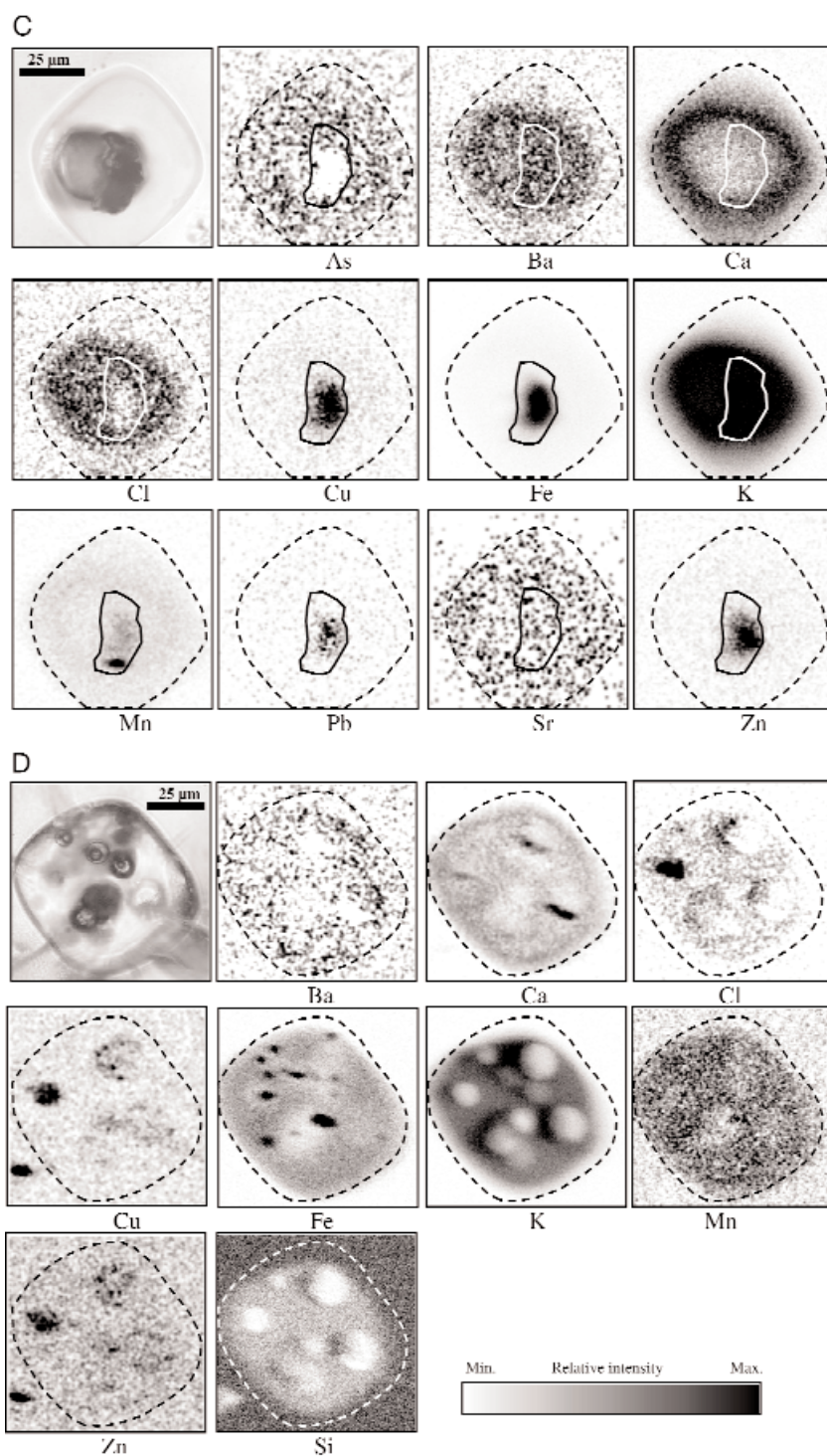
C

D

FIG. 4. *(Cont.)*

Composite inclusions

Microthermometric measurements on composite inclusions of glass and liquid in the samples of the La Copa rhyolite are made particularly difficult by metastability of the aqueous phases. In some single-phase liquid-filled bubbles (similar to those in Fig. 5A), metastable vapor bubbles appeared during freezing experiments and disappeared spontaneously after a random period (>5 min and <2 d). Metastability also was suggested by positive final ice-melting temperatures (T_m) up to 0.8°C. Roedder (1984, p. 298) referred to this phenomenon as "metastably superheated ice." A smaller number of liquid-filled bubbles had final ice-melting temperatures values between –5° and –14°C. Discounting the lower
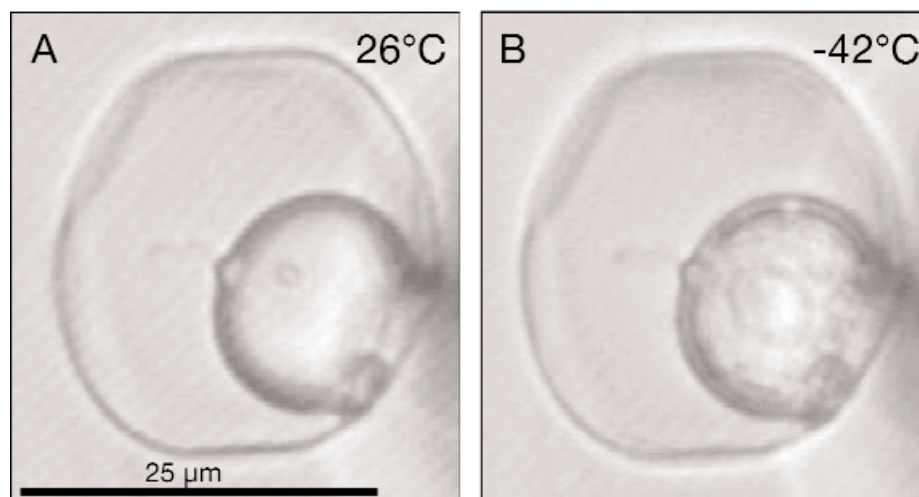
FIG. 5. Photomicrograph of a freezing experiment on a single-phase aqueous liquid-filled bubble in a glass inclusion in a quartz phenocryst from the La Copa lava (CA31). A. At room temperature. B. At –42°C. Note that the contents of the bubble have frozen to a mass of tiny ice crystals. The clear bubbles in Figure 3D show similar freezing behavior.

temperature range as a probable artifact of metastability and using the techniques of Bodnar and Vityk (1994), salinities of 13 to 17 wt percent $NaCl_{equiv}$ are estimated for these inclusions. However, it seems likely that salinities of primary magmatic fluids ranged from 13 wt percent $NaCl_{equiv}$ (one- or two-phase inclusions) to ≈40 wt percent $NaCl_{equiv}$ (halite-bearing inclusions, e.g. Fig. 3E). No homogenization temperatures could be determined from the rare composite inclusions of glass and liquid containing halite, as they inevitably decrepitated during heating experiments.

Inclusion Compositions

Silicate inclusions

Table 2 gives average compositions for glass inclusions from the La Copa samples. Totals less than 100 percent are considered to be reasonable approximations of the H_2O concentrations.

TABLE 3. Summary Homogenization Temperatures of Fluid Inclusions in Quartz Phenocrysts in Sample 9915 from the Don Luis Porphyry

Homogenization	Multiphase inclusions		Two-phase inclusions
	Halite disappearance (°C)	Bubble disappearance (°C)	Bubble disappearance (°C)
$T_{h(max)}$	>600	600	360
$T_{h(mean)}$	462	385	292
1σ	54	79	22
$T_{h(min)}$	340	165	260
$T_{h(mean)} + 1\sigma$	516	464	314
$T_{h(mean)} - 1\sigma$	408	306	270

Notes: The maximum recommended operating temperature for the Linkam THMS 600 stage is 600°C, a few inclusions were noted that retained a small amount of halite at 600°C, and homogenization is presumed to be by halite disappearance at 600° to 650°C

PIXE microprobe analyses were performed on crystallized silicate inclusions selected to represent a range from silicate- to vapor-rich (Table 4). Figure 4A is an example of the analysis of an inclusion with an intermediate vapor content, in which Ca, K, and Fe show strong enrichments but with spatial distributions that do not correspond with each other. The silicate component of crystallized silicate melt inclusions is an intimate but variable mix of Na- and K-feldspars, muscovite and quartz, and the PIXE element maps for Ca, K and Fe reflect this. In contrast, the lithophile elements, Zr, Ba, and Rb, are more evenly distributed within the outline of the inclusion, suggesting their mutual substitution in the crystallized silicates. The distribution of Cu, Pb, and Zn (plus Br, Fe, Rb, and Sr in some inclusions) is quite variable. In Figure 4A, these elements also show a general correspondence with the outline of the inclusion, implying mutual substitution in the silicates. In other examples elevated concentrations of Cu, Zn, and Pb are associated with small (<2-μm) solid phases, possibly sulfides (e.g., Fig. 4B). In others, Cu, Zn, and Pb apparently occur in trapped crystals of magmatic minerals, possibly as trace elements in Fe-Ti oxides. Davidson and Kamenetsky (2001) presented results of a qualitative LA-ICPMS analysis of a crystallized silicate melt inclusion, which showed that copper was mainly in the phase interstitial to the crystalline silicates (aqueous vapor ± liquid) or in tiny sulfide crystals.

PIXE element maps of primary vapor-rich magmatic inclusions (e.g., Fig. 4B) do not show a correspondence of Zr, Ba, Rb, or Sr with the outline of the inclusions, unlike silicate inclusions, and have much lower concentrations of K, Na, Fe, and Mn. This suggests that vapor-rich inclusions contain only small amounts of scattered silicate crystals, consistent with observations made by scanning electron microscopy of open inclusions (e.g., Fig. 2F). PIXE analysis of the inclusions (Table 4) shows that K concentrations in crystallized silicate melt inclusions vary between 7.3 wt percent, consistent with an inclusion containing >90 percent silicate with a bulk composition equivalent to the melt inclusion glasses and 0.76 wt

TABLE 4. Proton Induced X-Ray Emission Microprobe Analysis of Fluid Inclusions from the Don Luis Porphyry and Melt Inclusions from the La Copa Rhyolite (concentrations in ppm)

Analysis	Sample	Cl	K	Ca	Mn	Fe	Cu	Zn	Ga	As	Br	Rb	Sr	Zr	Ba	Pb
Fluid inclusions																
bm15	9915	358095	63788	6324	4154	43580	2128	1146	na	783	672	bd.	bd.	na	na	487
bm16	9915	10412	7251	1343	1430	34410	14152	883	na	1041	545	bd.	bd.	na	na	615
bm16b	9915	td	17112	16335	2264	34706	1112	1135	na	742	522	1082	bd.	na	na	bd.
bm17	9915	28739	12865	1997	3920	57828	694	1664	na	1855	861	1790	bd.	na	na	624
bm21a	9915	494045	109931	5202	6295	92952	9051	2725	bd.	2400	1350	2711	bd.	bd.	bd.	bd.
bm21b	9915	256316	76338	2979	4810	71902	1774	2056	bd.	650	1120	2383	bd.	bd.	bd.	bd.
Vapor-rich melt inclusions																
bm43	DC-Rhy1	2136	3374	579	141	17940	395	102	bd.	bd.	51	bd.	79	bd.	bd.	43289
Crystalline silicate melt inclusions																
bm36a	9903	td	73342	7903	362	5233	22	46	43	16	bd.	bd.	bd.	bd.	2350	bd.
bm36b	9903	td	72611	4110	332	5483	40	45	33	27	bd.	bd.	bd.	bd.	2553	bd.
bm18	9915	646	71953	2366	485	10601	55	96	63	67	bd.	332	362	274	3645	bd.
bm34	9902	td	45005	2937	617	11342	85	79	35	33	bd.	237	175	5031	1368	bd.
bm38	CA31	td	42530	4856	426	5896	31	43	27	bd.	17	128	117	99	45	68
bm31	9902	td	21147	6145	301	4565	44	63	36	56	bd.	bd.	215	bd.	2355	bd.
bm35	9903	td	15427	3214	527	10056	48	59	29	27	bd.	138	172	930	1409	bd.
bm32	9902	td	td	td	431	5979	73	92	53	34	bd.	243	219	346	2224	bd.
bm36c	9903	td	7628	1266	79	1541	76	28	14	16	bd.	bd.	123	<50	926	bd.
Composite inclusions																
bm42a	9902	1385	91213	5708	346	4503	14	40	40	36	bd.	164	bd.	bd.	1236	bd.
Glass + solid																
bm47	CA31	2928	29223	3438	238	2890	32	29	21	23	bd.	97	70	44	na	33
Glass + liquid																
bm48	CA31	83281	100440	34225	796	8830	164	141	39	45	bd.	248	243	152	na	178
Glass + liquid																

Notes: Analyses performed on the CSIRO-GEMOC nuclear microprobe at North Ryde in Sydney; data processed to give concentrations in ppm; td = no analysis because the inclusion was too deep, na = not analyzed, bd = below detection limit; note, detection limits for PIXE analyses are dependent on factors such as inclusion size and depth, and beam charge, and vary from inclusion to inclusion; composite inclusions are listed as glass + solid (i.e., glass + crystallized silicates) or glass + aqueous fluid; all analyses are for the whole inclusion; inclusions are listed with sample numbers as per Table 2

percent, equivalent to <10 percent silicates. From the available analyses, K and K/Mn appear to be good proxies for the silicate content of crystallized silicate melt inclusions and vapor inclusions. Figure 6 shows a trend to increasing metal concentration with decreasing silicate content, which strongly implies that metals are concentrated in the vapor-phase rather than in the coexisting melt.

Fluid inclusions

PIXE analyses of hypersaline fluid inclusions are given in Table 4. PIXE element maps show high concentrations of Na, K, and Ca in areas of the inclusion corresponding to crystals, indicating that they are halite, sylvite, and anhydrite. The aqueous liquid has intermediate concentrations of As, Br, Cl, Cu, K, Mn, Pb, Rb, and Zn and high concentrations of Fe. Measured concentrations of metals are generally high but variable (e.g., 700–14,000 ppm Cu and 900–3,000 ppm Zn). Similarly high concentrations of metals have been reported in fluid inclusions from mineralized quartz veins at Río Blanco (Frikken, 2004). Metal concentrations in liquid and vapor phase inclusions from the Don Luis Porphyry are consistently high and heterogeneous in composition typical of magmatic volatile phases (e.g., Kamenetsky et al., 2002, 2004).

Composite inclusions

PIXE element maps of typical composite inclusions of glass + crystallized silicates (Fig. 4C) show that the dark globules have element distributions distinct from those of either the glass or the shrinkage bubble. Notably they indicate higher concentrations of Cu, Fe, Ge, Mn, Pb, and Zn, typical of crystallized silicate melt inclusions (Table 4). The glass in composite inclusions, either glass + crystallized silicates (Fig. 4C) or glass + aqueous fluid (Fig. 4D), have concentrations of Ca, K, Fe, Mn, Rb, and Sr ± Ba that are consistent with aluminosilicate glass. The aqueous bubbles have variable compositions; some have low metal concentrations (presumably low-salinity metal-poor liquid or vapor), others are metal rich and have high salinities. In the PIXE element maps of some bubbles all elements are more concentrated in the glass or the inclusion host than in the bubbles, although others contain high

concentrations of Cl, Cu, Zn, and Fe. In some cases, the high concentrations correspond to the outline of the bubbles, suggesting that the metals are in solution at room temperature. In others, Cu, Zn, and Fe are concentrated within specific domains in bubbles, corresponding to the location of tiny opaque phases and suggesting the presence of magnetite and/or chalcopyrite crystals. Considerable heterogeneity is observed, but in general the liquid-filled bubbles have higher concentrations of metals than the glass. Similar heterogeneous compositions have been noted in bubbles within a single silicate melt inclusion in the Omsukchan Granite (Kamenetsky et al., 2004).

Discussion

Composite inclusions

There are two possible explanations for the composite inclusions that consist of bubbles of one- or two-phase aqueous liquid in silicate glass: postemplacement refilling of breached shrinkage bubbles or heterogeneous trapping of a coexisting melt and an aqueous fluid phase. In most examples, our petrographic observations do not support refilling. Translucent and opaque crystalline precipitates are noted in some of the clear liquid-filled bubbles (Fig. 3E), and microthermometric experiments yield salinities from 13 to > 40 wt percent $NaCl_{equiv}$. Additionally, PIXE data (Table 4) indicate elevated concentrations of Fe, Cu, and Zn in some liquid-filled bubbles, some possibly containing magnetite and sulfide crystals. The elevated salinities and high metal concentrations are more consistent with a magmatic rather than meteoric fluid and argue against postemplacement refilling. Further, the presence of rare primary fluid-only inclusions in the La Copa samples (e.g., Fig. 3A) implies that an aqueous fluid phase was present in the magma. Plastic deformation of some of the aqueous liquid-filled bubbles (e.g., Fig. 3D) is also consistent with syn- or posttrapping deformation of melt containing one or more bubbles of aqueous liquid. Shrinkage bubbles, on the other hand, are typically almost spherical (e.g., Fig. 2B), even in the inclusions with deformed liquid-filled bubbles (Fig. 3D). It seems improbable that selective refilling of only deformed bubbles has occurred. Instead, trapping of coexisting phases (silicate melt and aqueous fluid) is inferred to be the most likely mechanism of formation of the liquid-filled bubbles.

Although clearly demonstrated by analyses and microthermometry, the existence of single-phase aqueous bubbles inside melt inclusions appears inconsistent with normal cooling behavior of aqueous liquids. Under constant-volume conditions, cooling of an aqueous liquid from magmatic temperatures should produce a volume reduction, leading to the nucleation of a vapor bubble. However, the single-phase aqueous liquid bubbles might be explained by the physical properties of the host mineral and the inclusion. The bulk modulus of a trapped silicate melt is about one order of magnitude less than the elastic modulus of the host quartz. Therefore, differential expansion during decompression should put a silicate melt inside a quartz phenocryst under compression (Tait, 1992). The volume change associated with the α to β quartz transition at 573°C should further increase the pressure within a trapped melt inclusion. If compression
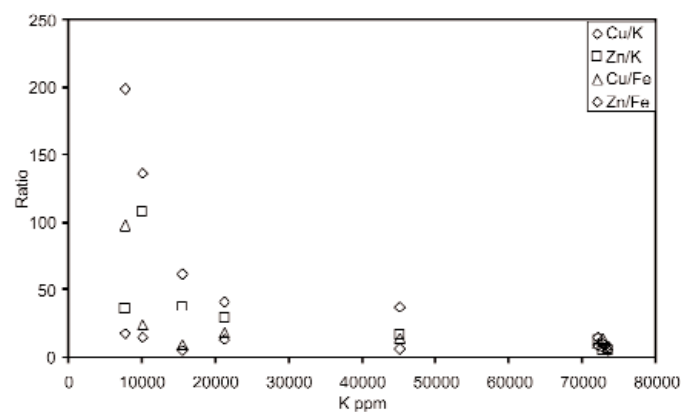

FIG. 6. Ratios of Cu/K, Zn/K, Cu/Fe, and Zn/Fe vs. K for crystallized silicate melt inclusions. K is used as a proxy for the silicate component of a crystallized silicate melt inclusion, high K corresponds to high aluminosilicate content (and correspondingly low vapor content). Data from PIXE analyses are listed in Table 4.

results in a volume reduction of an enclosed aqueous liquid bubble, equal to (or greater than) the volume reduction due to cooling of the aqueous liquid, then vapor bubble nucleation would be suppressed or already-formed bubbles may disappear.

Visually, such single-phase aqueous liquid bubbles differ from shrinkage bubbles only in that they have a silver-gray color in transmitted light, whereas shrinkage bubbles appear black (due to almost total internal reflection). Given the visual similarity to shrinkage bubbles, it may be that single-phase aqueous liquid bubbles in melt inclusions are more common than might be suggested by the few published examples (Naumov et. al. 1992, 1994).

Magmatic emulsions

In addition to one- or two-phase aqueous fluid-filled bubbles, some composite inclusions contain numerous tiny bubbles (10s to 100s, e.g., Fig. 3F) with a total volume typically much greater than the average of 6 ± 2 (1σ) vol percent, noted for shrinkage bubbles in the glass inclusions. Additionally the bubbles are of uniform size (in a given inclusion), and in some inclusions one- and two-phase liquid-filled bubbles occur randomly with the vapor bubbles and have similar sizes (Fig. 3F). None of these features are characteristic of shrinkage bubbles but are consistent with trapping of an emulsion of melt and a dispersed aqueous fluid phase.

Roedder (1984) proposed a simple but convincing test of magmatic immiscibility, namely the existence of an assemblage of melt inclusions showing trapping of variable proportions of the supposed immiscible phases. Post-trapping exsolution and/or crystallization of a phase tends to produce a constant phase ratio, whereas accidental trapping, by definition, does not (e.g., Kamenetsky et al., 2003). Figures 3D to F and 5A show variable phase ratios within composite inclusions containing liquid and vapor bubbles. This observation supports the contention that the aqueous fluids were immiscible with respect to the La Copa rhyolite magmas at the time of quartz crystallization.

Microthermometry and geologic reconstructions suggest that exsolution of a volatile phase(s) from the Río Blanco magma occurred at pressures below the critical pressure for H_2O (probably <0.5 kbar: Holmgren et al., 1988; Vargas et al., 1999). Modeling by Shinohara (1994) suggests that at pressures <1.3 kbars, any volatile phase exsolved from a felsic magma should be a low-salinity vapor with a small amount of hypersaline brine (1–3 wt %). Thus, exsolution could be expected to form a magmatic emulsion of tiny vapor bubbles (and rare brine-filled bubbles) surrounded by melt, as observed in Figure 3F. Given the rates of phenocryst growth demonstrated by Swanson and Fenn (1986), we consider it reasonable that the magmatic inclusions from the La Copa Complex could have formed rapidly enough to trap these short-lived, transient emulsions.

Magmatic emulsions within a melt are expected to be disrupted under the influence of gravity and continued bubble growth (Proussevitch et al., 1993). The rate of breakdown is dependent on bubble size, beginning slowly but speeding up when the bubbles pass a critical size (Proussevitch et al., 1993). Gradually, the bubbles coalesce, and the magmatic emulsion evolves into large discrete brine and vapor bubbles

that have separated from the melt. Thus, we might reasonably predict that magmatic inclusions that sampled different stages in the evolution of this system should have a wide range of liquid, vapor, and melt contents. This is consistent with the observation of variable aqueous fluid proportions in composite glass + liquid inclusions (Fig. 3D-F). We also note similar variability in the range of silicate contents in crystallized silicate melt inclusions, from >90 percent (i.e., silicate inclusions; Fig. 2D, E) to <10 percent (i.e., vapor inclusions; Fig. 2C, F).

To explain the range of silicate- to vapor-rich inclusions, we previously suggested that H_2O and silicate melt were completely miscible under the conditions existing in the Río Blanco magma (Davidson and Kamenetsky, 2001). Based on new observations in this study, we suggest that the range of crystallized silicate melt inclusions may represent trapping of a magmatic emulsion having some properties of a single phase but with variable proportions of melt and vapor bubbles. Magmatic emulsion textures that occur in the La Copa extrusive rhyolites were not observed in the intrusive units, but we suggest that the slow cooling rates of the intrusion probably destroyed such textures. Thus inclusions that trapped magmatic emulsions in magma that did not erupt crystallized to form the more vapor-rich silicate inclusions in the La Copa intrusions and the Don Luis Porphyry (Figs. 2F, 4A-B). In contrast, inclusions that were quenched during eruption preserved the emulsion textures (e.g., Fig. 3D-F).

Derivation of hydrothermal fluids from volatile-rich melts

Melt inclusions in both the La Copa rhyolite and the Don Luis Porphyry show consistent evidence of exsolution of a volatile phase, from melts now most closely represented by the contents of silicate inclusions. However, inclusions in the La Copa rhyolite show only minor evidence of trapping of an exsolved vapor-rich phase.

In contrast, the abundance of hypersaline fluid inclusions in the Don Luis Porphyry suggests that the phenocrysts coexisted with hypersaline metal-rich fluids over a temperature range of at least 850° to <500°C. We suggest that the higher temperature fluid inclusions represent ponding of a pocket of silicate crystal mush and hypersaline fluids, in which melt and primary fluids ± magmatic crystals were trapped as inclusions in phenocrysts growing in the fluid-rich crystal mush. Such a pocket could record magmatic conditions, similar to very early stage melt inclusion-bearing quartz veins documented by Harris et al. (2003) at Bajo de le Alumbrera, Argentina. As the pocket cooled, fracturing of the phenocrysts would permit the trapping of aqueous fluids at progressively lower temperatures. Under these conditions, there is little distinction between primary, pseudosecondary, and secondary fluid inclusions. We suggest that the mix of melt and fluid inclusions, some clearly primary and some containing magmatic crystals (apatite and zircons), is evidence of these processes.

These are the most important differences between the inclusions from the La Copa Complex and the Don Luis Porphyry. Both show evidence of exsolution of a volatile-rich phase, however, in the La Copa Complex the amount was small and/or it escaped from the magma. In the Don Luis Porphyry (at least in the sampled location) ponding of melt and hydrothermal fluids likely occurred during cooling.

The foregoing model should have consequences for metal transport, given the preferential partitioning of metals from silicate melts to coexisting aqueous fluids (e.g., Lowenstern et al., 1991; Candela and Piccoli, 1995). Figures 6 and 7 plot Cu against K for silicate and vapor inclusions from the La Copa rhyolite and hypersaline fluid inclusions from the Don Luis Porphyry. Cu, Zn, Fe, and K ratios are used to reduce the heterogeneity typical of hypersaline fluid inclusions (e.g., Kamenetsky et al., 2002, 2004), and potassium is used as a proxy for the aluminosilicate content of an inclusion (Table 2). The silicate inclusions show a slight trend to higher Cu with lower K (i.e., lower aluminosilicate content), and the fluid inclusions continue this trend to very high Cu concentrations at high K, in the case of fluid inclusions K serves as a proxy for total chlorides. The only primary magmatic vapor inclusion for which a PIXE analysis is available lies between the fields for crystallized silicate melt inclusions and fluid inclusions. Although the La Copa rhyolite and Don Luis Porphyry are separate bodies, whole-rock analysis shows that they are compositionally similar and comagmatic (Warnaars, 1985; Serrano et al., 1996; Vargas et al., 1999). Thus, the trends in Figure 7 are consistent with the partitioning of metals from the silicate melt to the aqueous phase.

We suggest that the inclusion population of the La Copa rhyolite intrusions also exsolved magmatic fluids but these were quickly lost from the magma (possibly by venting during eruption). If any mineralization had resulted, it would occur either in the roof rocks (subsequently removed by erosion) or in the wall rocks (e.g., where recent drilling has uncovered mineralization adjacent to the La Copa rhyolite). In contrast, hydrothermal fluids exsolved from the Don Luis Porphyry may have ponded, permitting some localized mineralization. The potential for this fluid to generate ore is supported by the presence of sulfides (pyrite and chalcopyrite) in the sample analyzed.

Conclusions

In this paper we document evidence that unmixing of volatile-rich melt produced magmatic emulsions and that the progressive disruption of these emulsions concentrated the

hydrothermal fluid phases coexisting with the La Copa and Don Luis Porphyry magmas. Analysis of these phases provides evidence of partitioning of metal from silicate melt into emulsions of metal-rich liquid and vapor phases, which may have condensed to form hypersaline hydrothermal fluids that ponded with silicate crystal mush.

The melt inclusions present in the La Copa rhyolite show exsolution of a volatile-rich phase but only limited evidence for trapping of a metal-rich vapor phase. Inclusions in the Don Luis Porphyry also show evidence both of volatile phase exsolution and ponding of metal-rich hydrothermal fluids. Thus, the whole of the Don Luis porphyry may be more prospective for mineralization, but only the wall or roof rocks of the La Copa rhyolite, consistent with the distribution of mineralization observed at Río Blanco.

Acknowledgments

REFERENCES

Atkinson, W.W., Souviron, A., Vehrs, T.I., and Faunes, A., 1996, Geology and mineral zoning of the Los Pelambres porphyry copper deposit: Society of Economic Geologists Special Publication 5, p. 131–155.
Bodnar, R.J., and Vityk, M.O., 1994, Interpretation of microthermometric data for H₂O-NaCl fluid inclusions, *in* DeVivo, B., and Frezzoti, M.-L., eds., Fluid inclusions in minerals: Methods and applications: Blacksburg, VA, Virginia Polytechnic Institute and State University, p.117–130.
Camus, F., 2002, The Andean porphyry systems: Hobart, CODES Special Publication 4, p. 1–38.
Candela, P.A., and Holland, H.D., 1984, The partitioning of copper and molybdenum between silicate melts and aqueous fluids: Geochimica et Cosmochimica Acta, v. 48, p. 373–380.
Candela, P.A., and Piccoli, P.M., 1995, Model ore-metal partitioning from melts into vapor and vapor/brine mixtures: Mineralogical Association of Canada Short Course, v. 23, p. 101–127.
Cannell, J., Cooke, D., Walshe, J., and Stein, H., 2005, Geology, mineralization, alteration and structural evolution of El Teniente porphyry Cu-Mo deposit: ECONOMIC GEOLOGY, v. 100, p. 979–1003.
Cline, J.S., and Bodnar, R.J., 1991, Can economic porphyry copper mineralization be generated by a typical calc-alkaline melt?: Journal of Geophysical Research, v. 96, p. 8113–8126.
Davidson, P., and Kamenetsky, V.S., 2001, Immiscibility and continuous felsic melt-fluid evolution within the Rio Blanco porphyry system, Chile: Evidence from inclusions in magmatic quartz: ECONOMIC GEOLOGY, v. 96, p. 1921–1929.
Deckart, K., Clark, A.H., Aguilar, C.A., and Vargas, R.R., 2005, Magmatic and hydrothermal chronology of the supergiant Rio Blanco porphyry copper deposit, Central Chile: Implications of an integrated U-Pb and Ar-Ar database: ECONOMIC GEOLOGY, v. 100, p. 905–934.
Frezzotti, M.L., 2001, Silicate-melt inclusions in magmatic rocks: Application to petrology: Lithos, v. 55, p. 273–299.
Frikken, P.H., 2004, Breccia-hosted copper-molybdenum mineralization at Río Blanco, Chile: Unpublished Ph.D. thesis, Hobart, Tasmania, University of Tasmania, 290 p.
Frikken, P., Cooke, D., Walshe, J., Skarmeta, J., Serrano, L., and Vargas, R., 2005, Sulfur isotope and mineral zonation in the Sur-Sur Breccia Complex,
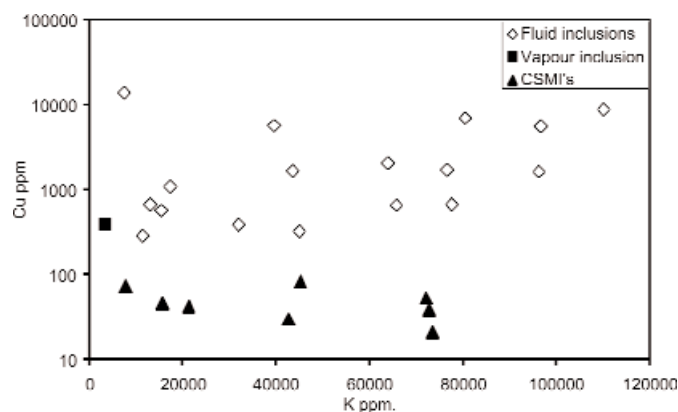

FIG. 7. Cu vs. K, for crystallized silicate melt inclusions and vapor and hypersaline fluid inclusions. Silicate inclusions show a slight trend to higher Cu with lower K (i.e., lower aluminosilicate content), fluid inclusions continue this trend to very high Cu concentrations at very high K. Data from PIXE analyses are listed in Table 4.

Rio Blanco Cu-Mo deposit, Chile—implications for ore genesis: Economic Geology, v. 100, p. 935–961.

Harris, A.C., Kamenetsky, V.S., White, N.C., Achterbergh, E.V., and Ryan, C., 2003, Melt inclusions in veins: Linking magmas and porphyry Cu deposits: Science, v. 302, p. 2109–2111.

Hedenquist, J.W., and Lowenstern, J.B., 1994, The role of magmas in the formation of hydrothermal ore deposits: Nature, v. 370, p. 519–527.

Hollings, P., Cooke, D., and Clark, A.H., 2005, Regional geochemistry of Tertiary igneous rocks in Central Chile: Implications for the geodynamic environment of giant porphyry copper and allied mineralization: Economic Geology, v. 100, p. 887–904.

Holmgren, C., Marti, M., Skewes, M.A., Schneider, A., and Harmon, y.R., 1988, Analysis isotopicos y de inclusiones fluidas en el yacimiento Los Bronces, Chile Central: V Congreso Geologico Chileno, Santiago, 1988, p. 299–312.

Kamenetsky, V.S., van Achterbergh, E., Ryan, C.G., Naumov, V.B., Mernagh, T.P., and Davidson, P., 2002, Extreme chemical heterogeneity of granite-derived hydrothermal fluids: An example from inclusions in a single crystal of miarolitic quartz: Geology, v. 30, p. 459–462.

Kamenetsky, V.S., De Vivo, B., Naumov, V.B., Kamenetsky, M.B., Mernagh, T.P., van Achterbergh, E., Ryan, C.G., and Davidson, P., 2003, Magmatic inclusions in the search for natural silicate-salt melt immiscibility: Methodology and examples: Developments in Volcanology 5, p. 65–82.

Kamenetsky, V.S., Naumov, V.B., Davidson, P., Achterbergh, E.V., and Ryan, C.G., 2004, Immiscibility between silicate magmas and aqueous fluids: A melt inclusion pursuit into the magmatic-hydrothermal transition in the Omsukchan Granite (NE Russia): Chemical Geology, v. 210, p. 73–90.

Lowenstern, J.B., 1995, Applications of silicate-melt inclusions to the study of magmatic volatiles: Mineralogical Association of Canada Short Course, v. 23, p. 71–99.

——2003, Bubbles and non-silicate fluids in melt inclusions: Developments in Volcanology 5, p. 143–148.

Lowenstern, J.B., Mahood, G.A., Rivers, M.L., and Sutton, S.R., 1991, Evidence for extreme partitioning of copper into a magmatic vapor phase: Science, v. 252, p. 1405–1408.

Morgan, G.B., VI., and London, D., 1996, Optimizing the electron microprobe analysis of hydrous alkali aluminosilicate glasses: American Mineralogist, v. 81, p. 1176–1185.

Naumov, V.B., Kovalenker, V.A., Rusinov, V.L., Solovova, I., and Kamen, M., 1992, High density fluid inclusions of magmatic water in phenocrysts from rhyolite of the Stiavnica stratovolcano (central Slovakia): Geologica Carpathica, v. 43, p. 85–89.

Naumov, V.B., Kovalenker, V.A., Rusinov, V.L., and Kononkova, N.N., 1994, Inclusions of high-density magmatic water in phenocrysts from acid volcanics of the western Carpathians and central Tien Shan: Petrology, v. 2, p. 480–494.

Proussevitch, A.A., Sahagian, D.L., and Kutolin, V.A., 1993, Stability of foams in silicate melts: Journal of Volcanology and Geothermal Research, v. 59, p. 161–178.

Roedder, E., 1984, Fluid inclusions: Reviews in Mineralogy, v. 12, 664 p.

Serrano, L., Vargas, R., Stambuk, V., Aguilar, C., Galeb, M., Holmgren, C., Contreras, A., Godoy, S., Vela, I., Skewes, M.A., and Stern, C.R., 1996, The late Miocene to early Pliocene Rio Blanco-Los Bronces copper deposit, central Chilean Andes: Society of Economic Geologists Special Publication 5, p. 119–130.

Shinohara, H., 1994, Exsolution of immiscible vapor and liquid phases from a crystallizing silicate melt: Implications for chlorine and metal transport: Geochimica et Cosmochimica Acta, v. 58, p. 5215–5221.

Swanson, S.E., and Fenn, P.M., 1986, Quartz crystallization in igneous rocks: American Mineralogist, v. 71, p. 331–342.

Tait, S., 1992, Selective preservation of melt inclusions in igneous phenocrysts: American Mineralogist, v. 77, p. 146–155.

Toro, J.C., 1986, Cuerpos subvolcanicos asociados a zonas de alteracion hidrothermal en la alta cordillera de Chile Central: Unpublished Memoria de Titulo, Departamento de Geosciencias, Antofagasta, Universidad del Norte, 174 p.

Vargas, R.R., Gustafson, L.B., Vukasovic, M., Tidy, E.F., and Skewes, M.A., 1999, Ore breccias in the Rio Blanco-Los Bronces porphyry copper deposit, Chile: Society of Economic Geologists Special Publication 7, p. 281–297.

Warnaars, F.W., Holmgren, C.D., and Barassi, S.F., 1985, Porphyry copper and tourmaline breccias at Los Bronces-Rio Blanco, Chile: Economic Geology, v. 80, p. 1544–1565.